On the validity of ion selective membrane simplification in concentration polarization

On the validity of ion selective membrane simplification in concentration polarization

Cite as: AIP Advances **11**, 035116 (2021); https://doi.org/10.1063/5.0037961
Submitted: 17 November 2020 • Accepted: 10 February 2021 • Published Online: 05 March 2021

Jiafei Jiang, Jing Tang, Bader Al-Anzi, et al.

On the validity of ion selective membrane simplification in concentration polarization

Cite as: AIP Advances 11, 035116 (2021); doi: 10.1063/5.0037961
Submitted: 17 November 2020 • Accepted: 10 February 2021 •
Published Online: 5 March 2021

Jiafei Jiang,[1,2,3,4] Jing Tang,[1,2,3,4] Bader Al-Anzi,[5] Jongyoon Han,[6] and Zirui Li[1,2,3,4,a)]

AFFILIATIONS

[1] State Key Laboratory of Reliability and Intelligence of Electrical Equipment, Hebei University of Technology, Tianjin 300401, China
[2] College of Mechanical and Electrical Engineering, Wenzhou University, Wenzhou 325000, China
[3] School of Mechanical Engineering, Hebei University of Technology, Tianjin 300401, China
[4] National Engineering Research Center for Technological Innovation Method and Tool, Tianjin 300401, People's Republic of China
[5] Department of Environment Technologies and Management, Kuwait University, P.O. Box 5969, Safat 13060, Kuwait
[6] Department of Electrical Engineering and Computer Science, Massachusetts Institute of Technology, Cambridge, Massachusetts 02139, USA

[a)] **Author to whom correspondence should be addressed:** lizirui@gmail.com

ABSTRACT

Ion selective membrane (ISM) is widely used in electrochemical engineering and micro-fluidic processes, yet accurate modeling of the ISM is still challenging due to many scientific issues. So far, assumptions on the "ideal ISM" have been used in most simulation studies involving ion transport and electrokinetic flow in ion concentration polarization systems, but the validity or accuracy of those assumptions has never been investigated. In this paper, using a two-dimensional nanochannel system with practical significance, we verify the validity of the ideal ISM model by making comparisons between the idealized ISM system and a more realistic permselective nanochannel system in terms of simplifications over the electrical potential, counter-ion concentration, and zero co-ion flux. Our results show that the simplifications of fixed voltage and fixed counter-ion concentration in the ideal ISM model are largely accurate in most situations, especially under high applied voltage and/or with high charge density inside the ISM. However, zero co-ion flux simplification is not exactly accurate in most occasions. Significant errors may be incurred by the zero co-ion flux assumption when steady state solutions are sought using the ISM model. Some discussions over the influences of structures of the nanochannel system are also added. The obtained results will help in obtaining detailed understanding of the transport features inside the nanoporous ISM, especially when the comparison between simulation and experimental data is necessary.

I. INTRODUCTION

Technologies involving the ion selective membrane (ISM) have developed steadily in past decades, especially in the fields of waste water treatment[1,2] and seawater desalination.[3,4] In recent years, ISMs' applications have extended to new technologies such as the fuel cell[5] and biomolecular preconcentration.[6,7] In these applications, ISMs are used to selectively transport ions of specific charges from one side of a membrane to the other side under an external electric field, while transport of ions of the opposite charge is blocked.[8] Fundamentally, this ion selectivity is originated from the charges on the solid phase of nanoporous material of the ISM.[9,10] More specifically, the charged groups on the solid surfaces of nanopores attract counter-ions in the solution (within the pores) and repel co-ions.[11] This phenomenon makes the number of counter-ions in the solution at the vicinity of the charged surfaces non-negligibly larger than that of co-ions, i.e., the solution there is charged. The thickness of this charged solution is characterized by the Debye length,[12] which is typically 1–10 nm for the dilute monovalent binary solution of 1–100 mol/m^3.[13] Because the sizes of pores

of the ISM are in nanoscale, the solution inside these pores contains a much larger number of counter-ions than co-ions. When an external electric field is applied, electric field driven flux of counter-ions is higher than that of co-ions. As a result, the number of counter-ions passing through the membrane is significantly higher than co-ions, and the membrane is functionally ion selective.[14] In an extreme situation, an ideal ISM permits only the passage of counter-ions, with all the co-ions blocked.[15]

As a typical application, ISMs have been utilized in electrodialysis (ED) for several decades.[16,17] In such systems, cations and anions in the solution are driven to move across alternately placed cation exchange membranes (CEMs) and anion exchange membranes (AEMs),[18,19] under the action of an external electric field. In a specific chamber, if the electric field is pointing to the CEM, cations will move in the direction of electric field and pass through the CEM. Meanwhile, anions will move in the opposite direction and then pass through the AEM. The result is that concentrations of both cations and anions in this chamber are lowered. During this process, concentrations of both cations and anions in the neighboring chambers are increased because the CEM and AEM in those chambers are placed such that the electric field driven motions of both cations and anions out of the chamber are blocked. The significant difference between ion concentrations on two sides of an ISM gives rise to a phenomenon of ion concentration polarization (ICP),[20–22] which will hinder the above-mentioned transport processes.

Traditionally, the current–voltage (I–V) curve has been regularly utilized to depict the ion transport behavior and the performance of ED systems.[23] It has been well established that I–V curves of ED and ICP systems can be largely divided into three distinct regimes when the voltage is increased.[24–26] In the Ohmic regime, the current increases linearly in the low voltage range. When the voltage is increased beyond a critical value, the current does not increase significantly with the voltage and the system enters the limiting current (LC) regime. If the voltage is further increased beyond another critical value, a sharp increase in current occurs and the system enters the overlimiting current (OLC) regime.[27,28]

A great number of theoretical studies have been conducted to reveal the ion transport mechanism behind the transport behaviors in these three regimes. The behaviors in Ohmic and LC regimes could be explained in terms of ion transport in stationary and neutral solutions.[29] In the Ohmic regime, more ions enter the membrane with the rise of voltage, resulting in the increasing current and decreasing ion concentration in the membrane–solution interface. If the membrane is ideally ion selective (the co-ion flux across the membrane is zero), the current is contributed solely by the diffusion of counter-ions. This trend continues until the ion concentration near the membrane surface is approaching zero, i.e., the ion depletion zone is formed. After that, the current will not grow with the voltage and the system enters the LC regime. Because the ion concentration in the proximity of the membrane is close to 0, and the resistance there is infinitely high, any increase in the voltage is absorbed there. Therefore, the number of ions getting into the membrane is unchanged. Rigorous theories of ion transport in Ohmic and LC regimes can be found in series papers of Rubinstein and Zaltzman's group.[30,31] Although the theory based on stationary fluid and electric neutrality gives a perfect explanation of the I–V relationship in Ohmic and LC regimes, it does not work in the OLC regime because it cannot explain the increase in current beyond the limiting current. Later studies showed that understanding I–V relationships in the OLC regime must include both intensive ion depletion and strong electroconvection of the fluid,[32–34] which results in the formation of vortices in the depletion zone. Due to the high-speed vortices, high concentration solution is brought into the membrane surface; thus, the total flux of the ions is significantly increased.[35,36] The formation of vortices has been experimentally demonstrated in the OLC regime.[37,38]

In most simulation studies involving ion transport and electrokinetic flow in the ICP system, assumptions for the "ideal ISM" have been used. In an ideal ISM model, the ISM is represented by a series of simplified boundary conditions at the ISM–ion solution interface: (I) fixed electric potential, (II) constant concentration of counter-ions, and (III) ideal ion selectivity, i.e., no flux for co-ions.[39–43] However, in view of the pore structure, which is inhomogeneous and not ideally ion selective, there exist doubts that how well these simplifications can reflect the actual ISM in operation of the experiments or industrial systems.[44,45] The validity of the above-mentioned simplification (I) requires high conductivity of the membrane. Otherwise, the resistance of the membrane will affect the distribution of actual voltage on the membrane–solution interface when the system is in operation. The boundary condition (II) requires high charge density inside the membrane, at least compared with that carried by co-ions in the solution outside the membrane.[46] If this is not true, both cations and anions will enter the nanopores. The existence of co-ions will change the counter-ion concentration inside the membrane, required by the neutrality condition. The boundary condition (III) requires a virtually zero concentration and/or nearly zero mobility of co-ions in the membrane; otherwise, the co-ion flux will not be negligible.[47] These requirements often may or may not be fulfilled in the actual system.

Therefore, it is important to know whether the ideal ISM simplifications are reflecting the key physics of the actual ISM in ICP systems. To answer these questions, we must go back to the microscopic structure of the membrane, i.e., nanometer scale pores with charged solid walls.[48–50] In practical terms, the nanochannel arrays with charged surfaces could be utilized to represent the actual ISMs to a great extent because widely used ISM materials such as Nafion® consist of a fluoropolymer network coordinated by sulfate charged groups, with an approximate pore size believed to be about 5 nm–20 nm.[51] Both nanochannels and membrane pores fulfill the function of ion selectivity but permit the existence of co-ions, although at lower concentrations. Essentially, arrays of nanochannels are suitable for representing the actual ISMs.

We conduct numerical analyses and make comparisons between two systems, one with the ISM replaced by simplified boundary conditions and the other with the ISM substituted by a series of parallel nanochannels with charged walls,[52] mimicking actual ion selective membrane nanopores (Fig. 1). Validity and accuracy of ideal simplifications applied on the ISM, such as fixed voltage, fixed counter-ion concentration, and zero co-ion flux, are analyzed based on the simulation results. In the end, we also conduct some study on the nanochannel system with different structure parameters in terms of the number and length of nanochannels.

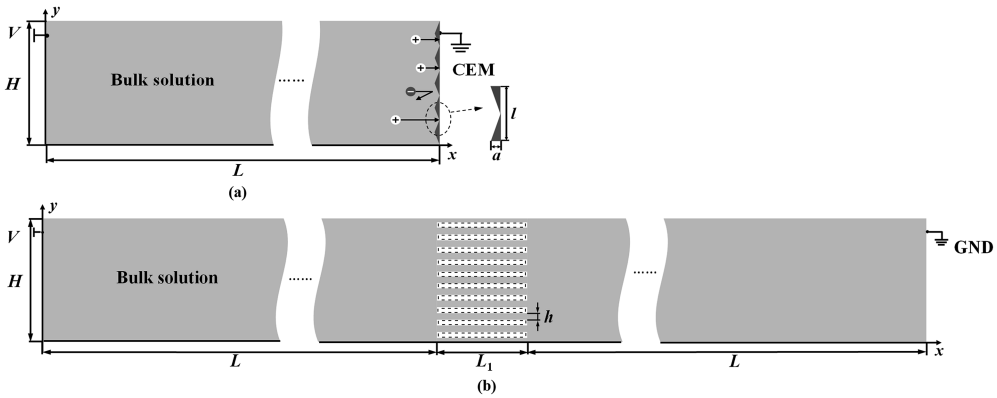

FIG. 1. Schematic of (a) the geometric model in the ideal ISM system and (b) the geometric model in the nanochannel system.

II. METHODS

A. Physical setup

Figure 1(a) shows the schematic of an electrokinetic model with the ideal homogeneous membrane. The system comprises a fluid domain of length L and height H. At the right end of the domain, a series of slightly wavy geometries are introduced to the CEM to represent the inhomogeneity of the nanoporous membrane surface. Each wavy unit of the membrane contains a linear variation of a distance l over a [see Fig. 1(a)]. The left boundary of the fluid domain is connected to a reservoir of potassium chloride (KCl) solution with concentration C_0. The electric potential is set to V on the left boundary, while the potential on the membrane surface is zero. For fluid flow, the left boundary of the fluid domain is set to be a dead-end (zero normal flow). On the membrane surface, the no-slip boundary condition is applied. This is because, in realistic membranes, water permeation through the membrane is extremely small and generally negligible, at least compared with other flow components in the system (i.e., tangential flow and/or secondary vortex-like flows). The upper and lower boundaries are periodic, making the computational domain represent a small portion of an infinitely large system (in the height direction).

Figure 1(b) shows the schematic of the nanochannel system, in which a series of n nanochannels are placed in the middle of the domain. Each nanochannel is of width of h and length L_1. The walls of nanochannels are negatively charged with surface charge density $-\sigma_-$. The dimension of the fluidic domain (length L and width H) on both sides of nanochannels is the same as that in Fig. 1(a). The left and right boundaries are connected to reservoirs of KCl solution of concentration C_0. The left boundary is applied a voltage V, and the right boundary is grounded. As in the membrane system shown in Fig. 1(a), the upper and lower boundaries are assumed to be periodic. Last, the leftmost and rightmost boundaries of the nanochannel system are both set to be dead-ends. These setups facilitate a direct comparison of the states and the behaviors of the two systems.

One may think that the electric field in the left part of the nanochannel system is significantly lower than that in the membrane system, which makes the direct comparison of the two systems questionable. It will be shown (in Sec. III B) that, under the same conditions, the electric field in the left fluid domain of the nanochannel system [Fig. 1(b)] is very close to that in the membrane system [Fig. 1(a)].

B. Governing equations

Electrokinetic flow of fluid, transport of ions, and distribution of electric potential are governed by the coupled Navier–Stokes equations, Nernst–Planck equations, and Poisson equation,[42]

$$\rho\left(\frac{\partial \mathbf{U}}{\partial t} + (\mathbf{U}\cdot\nabla)\mathbf{U}\right) = -\nabla P + \eta\nabla\cdot\nabla\mathbf{U} + \mathbf{E}\rho_e, \tag{1}$$

$$\nabla\cdot\mathbf{U} = 0, \tag{2}$$

$$\frac{\partial C_\pm}{\partial t} = -\nabla\cdot\mathbf{J}_\pm, \tag{3}$$

$$\mathbf{J}_\pm = -(D_\pm\nabla C_\pm + z_\pm(D_\pm F/RT)C_\pm\nabla\Phi) + \mathbf{U}C_\pm, \tag{4}$$

$$-\nabla\cdot(\varepsilon\nabla\Phi) = \rho_e. \tag{5}$$

In the Navier–Stokes equations describing the motion of incompressible fluid [Eqs. (1) and (2)], ρ is the density of the solution, $\mathbf{U} \equiv (u, v)$ is the velocity field, t is the time, P is the pressure, η is the dynamic viscosity coefficient, $\mathbf{E}$ is the electric field, and ρ_e is the free space charge density. In the Nernst–Planck equation describing ion transport [Eqs. (3) and (4)], $\mathbf{J}_+$ ($\mathbf{J}_-$), C_+ (C_-), D_+ (D_-), and z_+ (z_-) are the flux, concentration, free solution diffusion coefficient, and valance of K^+ and Cl^-, respectively. Φ is the electric potential, the negative gradient of which the electric field $\boldsymbol{E} = \nabla\Phi$. F, R, T are the Faraday constant, gas constant, and temperature, respectively. In the Poisson equation describing the electric potential distribution [Eq. (5)], the dielectric constant of the solution $\varepsilon = \varepsilon_0\varepsilon_r$, where ε_0 and ε_r are the vacuum permittivity and relative permittivity of the bulk solution. The charge density in Eqs. (1) and (5) is determined by the ion concentrations $\rho_e = e(z_+C_+ + z_-C_-)$, where e represents the elementary charge.

C. Boundary conditions

To solve the coupled governing equations above, boundary conditions of the ideal ISM system and the nanochannel system must be applied. The boundary conditions of these two systems are as follows.[53,54]

With reference to Fig. 1(a), at the left boundary of the ISM system ($x = 0$ nm), (i) the concentration of K^+ and Cl^- ions is fixed as C_0; (ii) the no-slip condition is applied to implement the dead-end effect; and (iii) the electric potential is set to V,

$$C_+ = C_- = C_0, \quad \mathbf{U} = \mathbf{0}, \quad \Phi = V. \tag{6}$$

In the wavy conditions on the right side of the domain ($x = L$), (i) the cation concentration is set to the value required for neutralizing negative charges in the CEM; (ii) penetration of anions is totally blocked; (iii) the membrane is impermeable to the fluid; and (iv) the electric potential Φ is zero,[55]

$$C_+ = C_m/z_+, \quad \mathbf{J}_- \cdot \mathbf{n} = 0, \quad \mathbf{U} = \mathbf{0}, \quad \Phi = 0. \tag{7}$$

Here, $\mathbf{n}$ is the normal vector perpendicular to the boundary pointing out of the fluid domain. C_m (>0) is the concentration of K^+ that is required to neutralize the fixed charge in the ideal CEM, i.e., $C_m = -\rho_{e,m}/F$, with $\rho_{e,m}$ (<0) being the charge density of the CEM.

At the upper ($y = H$) and lower ($y = 0$) boundaries, periodic continuity conditions for concentrations, potentials, fluid velocities, and fluxes are applied, i.e.,

$$C_\pm|_{y=H} = C_\pm|_{y=0}, \quad \Phi|_{y=H} = \Phi|_{y=0}, \quad \mathbf{U}|_{y=H} = \mathbf{U}|_{y=0}, \quad \mathbf{J}_\pm|_{y=H} = \mathbf{J}_\pm|_{y=0}. \tag{8}$$

As for the nanochannel system, the boundary conditions at the left, upper, and lower boundaries of the left domain to the nanochannels are the same as those in the ideal ISM system [Eqs. (6) and (8)]. In addition, settings of other boundary conditions in the nanochannel system shown in Fig. 1(b) are as follows.

At the right boundary in the nanochannel system ($x = 2L + L_1$), (i) the KCl solution is fully mixed with concentration C_0; (ii) the membrane surface is impermeable to the fluid; and (iii) the electric potential Φ is zero,

$$C_+ = C_- = C_0, \quad \mathbf{U} = \mathbf{0}, \quad \Phi = 0. \tag{9}$$

At the walls of nanochannels ($x = L \sim L + L_1$), (i) neither anions nor cations can pass through the walls; (ii) the no-slip condition is for the fluid flow; and (iii) the surfaces are negatively charged with density σ_- (<0),

$$\mathbf{J}_\pm \cdot \mathbf{n} = 0, \quad \mathbf{U} = \mathbf{0}, \quad \sigma = \sigma_-. \tag{10}$$

Due to the fact that the volumetric charge of the CEM comes from the negative surface charges on the walls of nanochannels in the unit volume, the membrane charge density $\rho_{e,m}$ and surface charge density σ_- must satisfy $\rho_{e,m}H = 2n\sigma_-$, i.e.,

$$\sigma_- = \rho_{e,m}H/2n = -FC_mH/2n. \tag{11}$$

Here, charges on the vertical walls of nanochannels are neglected.

D. Numerical methods

The governing equations [Eqs. (1)–(5)] with boundary conditions [Eqs. (6)–(10)] are solved using commercial software COMSOL v5.2a. Standard modules of Single-Phase Flow, Electrostatics, and Transport of Diluted Species are chosen to describe the laminar flow, electric potential distribution, and ion transport in both ISM and nanochannel systems. The computational domains are discretized into quadrilateral meshes. For the sake of describing the highly nonlinear nature of the ion concentration near the CEM and the charged walls of nanochannels, extremely fine meshes are adopted at these locations. At least three layers of elements are required within one Debye length from surfaces of membrane or walls of nanochannels. The Debye length is given by

$$\lambda_D = \sqrt{\frac{\varepsilon k_B T}{2(ze)^2 C_0}}. \tag{13}$$

Coupled governing equations are solved by MUMPS with Newton's method. In particular, we seek steady-state solutions, which describe the system state after the system runs for sufficiently long time. To obtain a converged solution under particular conditions, or to study the effect of specific parameters, auxiliary sweep of parameters is frequently used.

III. RESULTS AND DISCUSSIONS

With reference to the membrane model in Fig. 1(a), we conduct numerical simulation of the ideal ISM system with geometric parameters $H = 40$ nm, $L = 2000$ nm, $a = 0.2$ nm, and $l = 8$ nm, respectively. The concentration of bulk KCl solution is $C_0 = 1$ mol/m^3. Valence diffusion coefficients of K^+ and Cl^- ions are $z_+ = 1$, $z_- = -1$, $D_+ = 1.957 \times 10^{-9}$ m^2/s, and $D_- = 2.032 \times 10^{-9}$ m^2/s, respectively. The density, viscosity, and relative permittivity of the solution are $\rho = 1000$ kg/m^3, $\eta = 0.001$ Pas, and $\varepsilon_r = 78.5$, respectively. The absolute temperature is fixed at $T = 300$ K.

For the nanochannel system model as shown in Fig. 1(b), the geometric parameters (H and L) are the same as those in the ideal ISM system. The bulk concentration (C_0), transport parameters of ions (D_+, D_-), hydrodynamic parameters (ρ, η), and dielectric permittivity (ε_r) are also exactly the same as those in the membrane model as described above. Geometric parameters specific to the nanochannels are $L_1 = 500$ nm, $h = 2$ nm.

In the process of discretization, the sizes of elements in the direction perpendicular to the charged nanochannel walls are in geometrical sequence with the varied number of elements and element ratio. This meshing technique ensures that there are enough elements in the Debye layers near the channel wall or the depletion zones near ISM surfaces, and the total number of elements and the element quality are manageable in the solving stage. For example, in the vertical direction, the height of one of the nanochannels [h, see Fig. 1(b)] is discretized into ten elements, the sizes of which are in geometric sequence with symmetric distribution. The ratio of the maximum element size to the minimum size is 30. The minimum grid size is 0.02 nm, which is much lower than the Debye length of KCl of $C_0 = 1$ mol/m^3 at T = 300 K (~9.6 nm). Similarly, in the horizontal direction, the nanochannel domain ($x = L \sim L + L_1$) is discretized into 40 elements in

geometric sequence with symmetric distribution. The ratio of the maximum size to the minimum one is 25, with the minimum size of 0.32 nm.

We start with a typical nanochannel system and its corresponding ideal ISM system to check whether the ideal ISM simplifications are qualitatively describing the key physics of nanochannels. Later, we will assess the accuracy of the ideal ISM boundary conditions under varied electric fields, membrane charge densities, lengths of nanochannels, etc.

A. Qualitative comparison between ideal ISM system and nanochannel system

In order to test the validity of the ideal ISM treatment, the behaviors of ion and fluid transport in two models are shown in Fig. 1. In addition to the parameters described above, we choose $C_m = 16C_0$ (16 mol/m^3) in the ideal ISM model with the membrane charge density corresponding to the surface charge density of $\sigma_- = -3.087$ mC/m^2 in the nanochannel system of $n = 10$. The voltage applied on the left boundaries of both systems is $V = 30V_T$ ($V_T = k_BT/e = 25.8$ mV is the thermal voltage and k_B is the Boltzmann constant). We will compare the steady state distribution of concentrations and the I–V curves of both systems. The current density I is calculated through the average flux across the cross section in the y direction,

$$I = F\int_0^H (J_{+,x} - J_{-,x})dy/H. \tag{12}$$

Here, $J_{+,x}$ and $J_{-,x}$ are the x-component of $\mathbf{J}_+$ and $\mathbf{J}_-$, respectively. It is noteworthy that, at the steady state, I is constant at all locations in the x-axis due to mass conservation.

Figure 2(a) shows the distribution of C_- (solid line) and C_+ (dashed line) along the horizontal line ($y = 20$ nm) in the ideal ISM system and left domain of the nanochannel system, respectively. It could be found that, at $V = 30V_T$, distributions of ion concentrations are quite similar. Significant ion depletion takes place in both systems because concentrations of both K^+ and Cl^- are close to zero near the membrane surface [in Fig. 1(a)] or nanochannel interface [in Fig. 1(b)]. The length of the extended space charge (ESC) layer,[56] where the concentration of K^+ is non-negligibly higher than that of Cl^-, is around 500 nm, which is ~50 times higher than λ_D. Outside the ESC, there is an electroneutral domain called the diffusion boundary layer (DBL), characterized by a linear decrease in equal concentrations of both K^+ and Cl^- ions. Although there are slight differences between the exact values of the corresponding concentrations in the depletion region, these two systems produced the same physics qualitatively. In this sense, the ideal membrane model represented by the boundary conditions in Eq. (7) is capable of providing the essential permselective functionalities of the nanoporous ISM.

Figure 2(b) shows the comparison of I–V curves between the ideal ISM system and the nanochannel system. It could be seen that the current densities of both systems grow linearly at a high rate at low voltages (in the Ohmic regime) and the currents grow at a much slower rate beyond a certain voltage, when the system enters the LC regime. Meanwhile, it can be clearly found that the voltage of the transition (between the Ohmic regime and the LC regime) is almost the same in two systems ($V \sim 10V_T$). These results demonstrate that both systems produce the Ohmic and LC regimes of I–V relationship,[23,24] although the values of I in the nanochannel system are slightly higher than those in the ideal ISM system. Therefore, the ideal ISM model is able to produce key ionic transfer features of the nanoporous membrane, at least qualitatively.

Despite the qualitative agreement, there are some apparent quantitative differences between the results from the two systems: both the ion concentrations and the electric currents of the ideal ISM system are lower than their counterparts in the nanochannel system. This is because the nanochannel system permits passage of co-ions, which compromises the ion depletion effect and contributes additional electric current, as compared with the ideal ISM system. It is also unexpected that the ideal ISM system produces negative current when the voltage is lower than $3V_T$, which is an error intrinsic in the ideal ISM. In fact, this is because of the negative diffusive flux from the membrane (with fixed $C_+ = 16C_0$ on the CEM at $x = L$ and $C_+ = C_0$ on the left boundary at $x = 0$). This diffusive flux is not present in the nanochannel system because the highly concentrated counter-ions are attracted by the fixed charges on the solid channel wall. Counter-ions are not able to diffuse freely to the left boundary with low concentration.

In Secs. III B–III D, we will discuss the validity of three simplifications in the ideal ISM: fixed voltage, fixed counter-ion concentration, and zero co-ion flux, respectively. Later, the effects of nanochannel geometries, namely, the number of nanochannels (within a total height H) and the length of nanochannels, will also be elaborated.

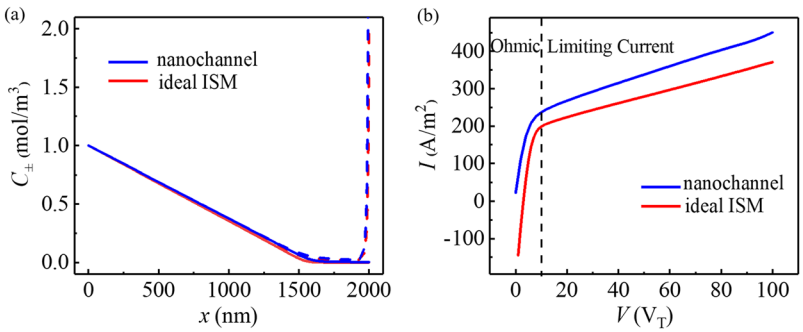

FIG. 2. (a) Distribution of C_- (solid line) and C_+ (dashed line) along the horizontal line ($y = 20$ nm) at $C_m = 16C_0$ and $V = 30V_T$ in the ideal membrane system and nanochannel system. (b) Comparison of I–V curves of ideal membrane and nanochannel systems at $C_m = 16C_0$.

B. Validity of fixed voltage on ideal membrane

In our ideal membrane model, and almost all the existing studies,[20,21,41] fixed voltage is directly applied on the membrane surface [$\Phi = 0$ in Eq. (7)]. However, in the actual implementation, the fixed voltage must be applied on the other side of the membrane in the presence of ion solutions. From the modeling point of view, it is essential to know the actual electric potential at the surface of the membrane and how it is affected by the properties of the membrane and the existence of solutions on the other side. In this work, when parallel nanochannels as shown in Fig. 1(b) are used to represent the nanoporous ISM in Fig. 1(a), we want to know the voltage value at the left boundaries of nanochannels and whether it corresponds to that applied to the ideal ISM. If the actual voltage at the left boundary of the nanochannels deviates from that applied on the ISM significantly, the fixed electric potential of ideal ISM simplification is not accurate.

For this purpose, we calculate the average electric potential (V_A) at location $2\lambda_D$ from the CEM and nanochannels ($x = L - 2\lambda_D$). Because λ_D of 1 mol/m^3 KCl solution is less than 10 nm, the voltage at $x = L - 2\lambda_D$ is close to the values at the CEM surface or nanochannel–solution interface, without significant impacts of the wavy geometry in the membrane model or the surface charges on the nanochannel walls.

Figure 3(a) shows the curves of V_A/V as V ranges from $0V_T$ to $100V_T$ in the ideal ISM system and nanochannel system, respectively. These two curves are very close to each other under voltage $V > 5V_T$, meaning that the fixed voltage treatment in the ideal ISM model is quite accurate in the LC regime [cf. Fig. 2(b)]. However, in the Ohmic regime, especially under $V < 5V_T$, the ideal ISM system overestimates the electric potentials near the membrane surface than that in the vicinity of the solution–nanochannel interface.

Figure 3(b) shows the electric potential distributions along a horizontal line ($y = 20$ nm) of the nanochannel system at $V = 5V_T$, $30V_T$, and $100V_T$, respectively. It could be clearly found that the voltage drops in the domain on the right side of nanochannels are significantly lower than those on the left side. To apply the full voltage drop on the left side of the membrane in the ideal ISM system is acceptable. In addition, the potential at the left boundary of nanochannels is close to zero, meaning that the treatment of fixed voltage at the membrane surface is valid.

It should be noted that the electric potentials inside the nanochannel region are lower than those in the adjacent solution. This drop of electric potential corresponds to the Donnan potential contributed by the negative charges on the walls of nanochannels.[11]

C. Validity of fixed counter-ion concentration inside the membrane

In our ideal membrane model, fixed counter-ion concentration $C_+ = C_m/z_+$ is applied on the CEM [cf. Eq. (7)], meaning that charges carried by counter-ions are equal to those by the membrane.[46] Here, we check this relationship using varied C_m (by modifying σ_-) under different V. Because the nanochannel region includes both solid and fluid phases, the apparent concentrations of K^+ and Cl^- in the nanochannel region are calculated through

$$\overline{C}_\pm = \int_L^{L+L_1} \int_0^H C_\pm dydx/HL_1. \tag{14}$$

Figure 4(a) shows the changes in $\overline{C}_+$ and $\overline{C}_-$ in the nanochannel region with the increase in C_m at $V = 30V_T$. It is obvious that the counter-ion concentration $\overline{C}_+$ (depicted by the red curve) is very close to C_m (depicted by the green line) when C_m is significantly higher than C_0. In this scenario, the apparent concentration of co-ions $\overline{C}_-$ (depicted by the blue line) is close to 0. In this scenario, the membrane boundary condition of fixed counter-ion concentration is accurate. However, when C_m is lower than $2C_0$, there are significant differences between $\overline{C}_+$ and C_m, which could be clearly depicted by the ratio of these two values in the inset. The reason accounting for the increase in $\overline{C}_+$ in low C_m situations is the non-negligible concentration of co-ions. The electric neutrality condition in the nanochannel region requires that $\overline{C}_+ = C_m + \overline{C}_-$. If C_m is low, the repulsive force applied to the co-ions from the fixed charge on the channel surfaces is not strong enough to exclude co-ions outside the nanochannels, and then the concentration of co-ions will become non-negligible. As a result, both $\overline{C}_+$ and $\overline{C}_-$ will be increased with their difference equal to C_m. It is noteworthy that, at $C_m = C_0$, $\overline{C}_+$ is 1.339 mol/m^3 (i.e., $1.339C_0$) and the relationship $\overline{C}_+ = C_m$ definitely does not hold. At $C_m = 2C_0$, which is commonly adopted in the existing literature,[19,37] $\overline{C}_+$ is 2.210 mol/m^3, which is 10.5% higher than the value defined by $\overline{C}_+ = C_m$.

Figure 4(b) shows the distributions of $\overline{C}_+$ and $\overline{C}_-$ inside the nanochannels, as V increases from 0 to $100V_T$ at $C_m = 2C_0$ and $C_m = 16C_0$. It could be clearly found that $\overline{C}_+$ is significantly higher than $\overline{C}_-$ in all voltage ranges; the differences between them are equal to C_m. The four curves are all basically flat as V increases, meaning

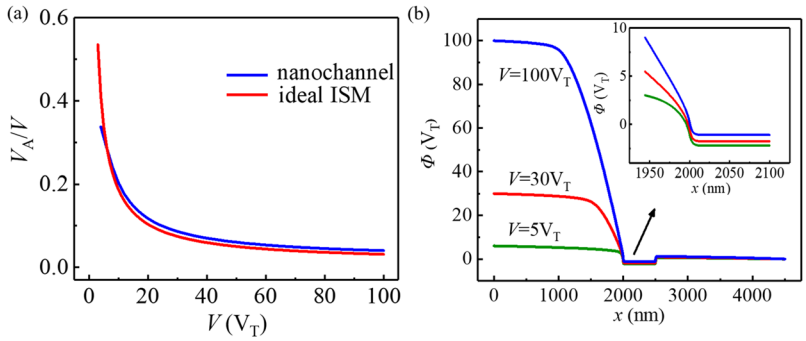

FIG. 3. (a) Comparison of the ratio of the average electric potential V_A to the applied voltage V at $x = L - 2\lambda_D$ in the ideal ISM and nanochannel systems. (b) Distribution of electric potential along the horizontal line ($y = 20$ nm) of the nanochannel system at different voltages.

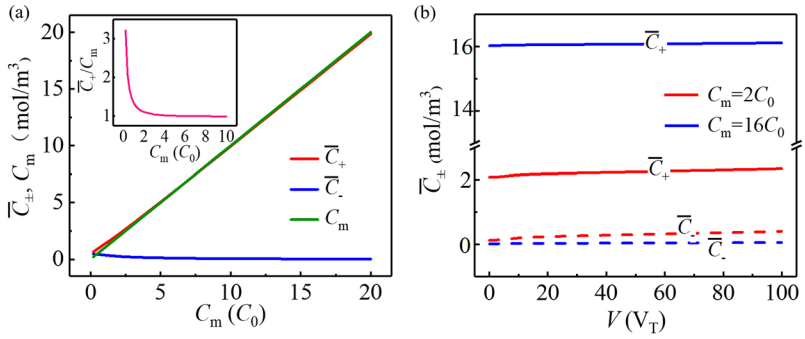

FIG. 4. (a) Dependence of $\bar{C}_+$ and $\bar{C}_-$ on C_m at V = 30V_T. (b) Dependence of $\bar{C}_+$ (solid line) and $\bar{C}_-$ (dashed line) on V at different C_m.

that the fixed counter-concentration simplification is largely valid and is insensitive to the electric field.

Based on these results, we may conclude that as long as C_m is much higher than C_0 (e.g., $C_m \geq 5C_0$), the simplification of the fixed counter-ion concentration is quantitatively accurate.

D. Validity of zero co-ion flux passing through the membrane

In the ideal membrane model, the ideal simplification of zero co-ion (Cl^-) flux across the membrane [Eq. (7)] is applied on the CEM. To test the validity of this simplification, we calculate the average fluxes of ions through nanochannels,

$$\bar{J}_{\pm} = \int_0^H J_{\pm,x} dy/H. \tag{15}$$

It is noteworthy that the values of $\bar{J}_+$ and $\bar{J}_-$ are constant at all vertical cross sections in the x-axis at the steady state. This is required by mass conservation. Because $\bar{J}_+$ and $-\bar{J}_-$ give positive contribution to the electric current, we will present the flux of Cl^- in the form of $-\bar{J}_-$. In addition, we define the permselectivity of nanochannels as the ratio of the counter-ion flux to the total flux, i.e.,

$$\gamma = \bar{J}_+/(\bar{J}_+ - \bar{J}_-). \tag{16}$$

If the nanochannels are highly permselective, the value of γ should be close to 1.

Figure 5(a) shows the distribution of $-\bar{J}_-$ and $\bar{J}_+$ with varied C_m at V = 30V_T. It can be found that the fluxes of both counter-ions and co-ions passing through the nanochannel decrease with C_m.

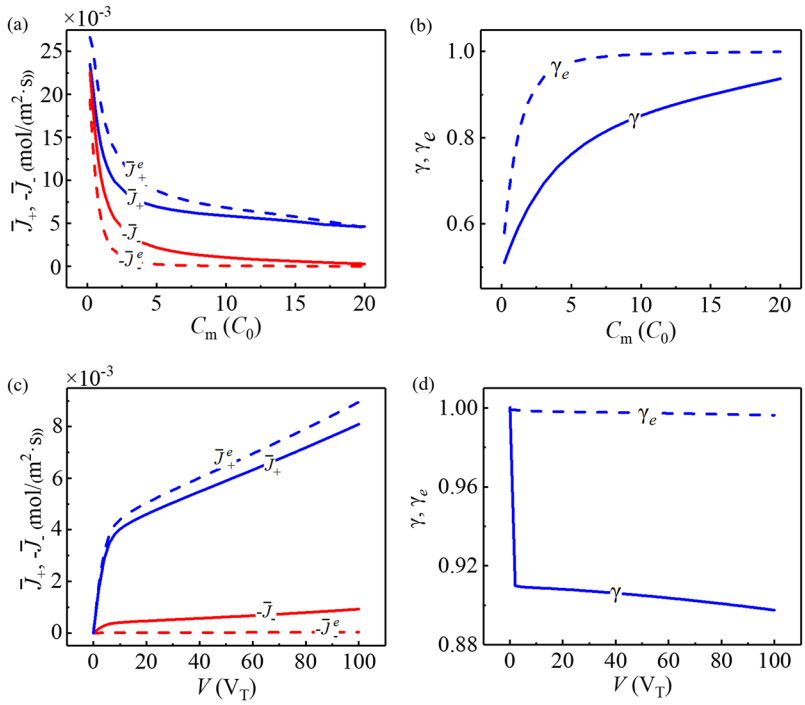

FIG. 5. (a) Dependence of ion fluxes on C_m in the nanochannel system. (b) Dependence of permselectivity γ on C_m. (c) Changes in ion fluxes under varied voltage V. (d) Changes in permselectivity under varied V.

Although the decrease in $-\bar{J}_-$ could be easily explained by enhanced exclusion of co-ions in nanochannels, the decrease in $\bar{J}_+$ is not straightforward. One may think that $\bar{J}_+$ should increase with C_m because the K^+ concentration inside the nanochannels is increased. However, the fact is $\bar{J}_+$ becomes lower because of stronger ion depletion and backward diffusion. More specifically, higher C_m reduces Cl^- transport from the right side of nanochannels to the left side and makes the concentration of Cl^- lower near the left boundary of nanochannels. The lowered Cl^- concentration at that location reduces the concentration of K^+ and makes the electrophoretic fluxes of K^+ across the nanochannels $\bar{J}_+^e$ lower [see the dashed curve in Fig. 5(a)].

As shown in Fig. 5(b), the permselectivity γ rises as C_m increases. This is in good agreement with our expectations. However, if we look at the values of permselectivity, which ranges from 0.576 at $C_m = 2C_0$ to 0.937 at $C_m = 20C_0$, we may find these values are unexpectedly lower than the actual ISM used in the industry. In fact, this is because these data are obtained in the steady state, which maximizes the co-ion fluxes and minimizes the counter-ion fluxes. If we use only the electrophoretic fluxes ($\bar{J}_+^e$ and $\bar{J}_-^e$) to calculate permselectivity (γ_e), it will range from 0.579 to 0.999 [see the dashed curve in Fig. 5(b)]. It is noteworthy that this treatment corresponds to a scenario with equal ion concentrations on both sides of the nanochannels because the convective flux caused by the fluid flow inside nanopores or nanochannels is ignored in both the actual membrane and our simulation model. In this situation, the permselectivity is close to 1.0 when C_m is higher than $5C_0$. The two curves in Fig. 5(b) give the selectivity of the nanochannel system under two states. The dashed one (γ_e) describes the selectivity of the system at a starting time, i.e., the concentration of ions on two sides of the nanochannels is equal, while the solid curve (γ) gives the selectivity at the ultimate, steady state, i.e., after the system runs for sufficiency long time. In the actual engineering systems, the permselectivity will start with γ_e and approaches γ as the selective ion transport proceeds and ion concentration polarization develops.

Figure 5(c) shows the distribution of co-ion flux $-\bar{J}_-$ and counter-ion flux $\bar{J}_+$ with the increase in V at $C_m = 16C_0$.. Both $\bar{J}_+$ and $-\bar{J}_-$ increase with V, and the increasing rate is significantly higher in the Ohmic regime than that in the LC regime. If we look at the value of $-\bar{J}_-$, we found it is significantly lower than $\bar{J}_+$. This means that the treatment of zero co-ion flux is qualitatively valid, at least significantly lower than the counter-ion flux. Again, if we look at the electrophoretic flux only (corresponding to the system without concentration difference on two sides of the nanochannels), the co-ion flux is very close to zero under $V < 100V_T$.

Figure 5(d) shows the changes in the permselectivity γ with the increase in V at $C_m = 16C_0$. It can be clearly found that γ is deteriorating as a function of applied voltage, which resulted in stronger concentration polarization and increased diffusive fluxes. In the Ohmic regime ($V < 4V_T$), the decreasing rate of selectivity (from 1.0 to 0.909) is much faster than that in the limiting current regime. If the ion concentrations on two sides of the nanochannels are equal, the selectivity γ_e is close to 1.0 under all voltages considered [see the dashed curve in Fig. 5(d)].

From the above results, we may conclude that the zero co-ion flux condition is accurate conditions of (1) $C_m > 5C_0$ and (2) the fact that concentration polarization is not significant. The deterioration of permselectivity under strong ICP has been observed repeatedly in the industrial processes. Here, we find that it is not because of the lowered selectivity of the membrane but because of the increased diffusive flux caused by the strong concentration polarization.

E. Effects of the width and the length of nanochannels in nanochannel system

Performances of the membrane are affected by the sizes of the nanopores and the thickness of the membranes. However, in the ISM model, with the membrane simplified as a permselective boundary, these parameters are completely ignored. In our nanochannel system, the size of nanopores is represented by the height h and the thickness of the membrane is represented by the length (L_1). To study the effects of these parameters, we fix the porosity (nh/H) and the charge density of membranes ($C_m = -2n\sigma_-/FH$) and calculate the I–V curves and the permselectivities of the system with varied h and L_1.

Figure 6(a) shows the comparison of I–V curves with 2, 5, 10, and 20 nanochannels at $C_m = 16C_0$. The widths of the single nanochannel in these systems are $h = 10$ nm ($\sim 1\lambda_D$), $h = 4$ nm ($\sim 0.4\lambda_D$), 2 nm ($\sim 0.2\lambda_D$), and 1 nm ($\sim 0.1\lambda_D$), respectively. It could be found that the currents are generally independent of the nanochannel width (pore size) as long as the membrane charge and the porosity are fixed. The current of $h = 10$ nm under $V = 100V_T$ is only 6.341% higher than that of $h = 1$ nm. We may conclude that the pore sizes have insignificant effect on the ion transport performance, as long as the pore sizes are smaller than the Debye length.

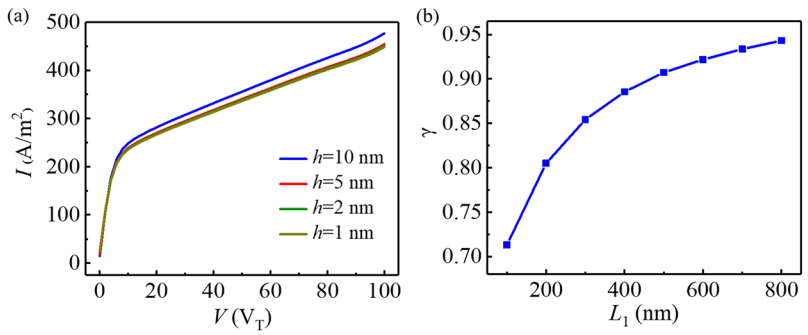

FIG. 6. (a) Comparison of I–V curves of the system with different numbers of nanochannels. (b) Dependence of permselectivity on the length of nanochannels.

Figure 6(b) shows the dependence of permselectivity and the length of nanochannel size L_1 at $C_m = 10C_0$ and $V = 30V_T$. It is clear that the value of γ gradually increases when L_1 increases from 100 nm to 800 nm. This means the permselectivity of the membranes will increase with membrane thickness, approaching 1.0 when the membrane is sufficiently thick.

F. Comparison of KCl and NaCl solutions

So far, our simulation is based on KCl solution. One may ask if the above results are valid to the electrolyte solution of other counter-ion types. To answer this question, we repeated our simulations with the same parameters but with K^+ ($D_+ = 1.957 \times 10^{-9}$ m^2/s) replaced by Na^+ ($D_+ = 1.334 \times 10^{-9}$ m^2/s) and compared the results relevant to the validity of the ideal ISM model. We found that the distribution of electric potential, concentration of counter-ions, and values of permselectivity of NaCl solution are basically the same as those of KCl solution. For example, at $C_m = 16C_0$ and $V = 20V_T$, the value of V_A/V of NaCl solution is 0.120, which is exactly the same as that of KCl. The concentrations of Na^+ ($\overline{C}_+ = 31.735$ mol/m^3) and Cl^- ($\overline{C}_- = 0.058$ mol/m^3) using NaCl solution are very close to their corresponding values ($\overline{C}_+ = 31.759$ mol/m^3 and $\overline{C}_- = 0.059$ mol/m^3). As for the permselectivity, the value of γ of NaCl solution ranges from 0.553 at $C_m = 2C_0$ to 0.926 at $C_m = 20C_0$, while the γ value of KCl solution ranges from 0.576 at $C_m = 2C_0$ to 0.937 at $C_m = 20C_0$ using KCl solution.

The conclusion that C_m is much higher than C_0, the simplification of the fixed counter-ion concentration that is quantitatively accurate, also applies in NaCl solution. In addition, when considering the average fluxes of ions through nanochannels in NaCl solution, the value of permselectivity γ ranges from 0.553 at $C_m = 2C_0$ to 0.926 at $C_m = 20C_0$, while γ changes from 0.576 to 0.937 when C_m changes from $2C_0$ to $20C_0$. These results show that all the conclusions about the validity of the ISM model are qualitatively the same in NaCl and KCl solutions.

IV. CONCLUSIONS

In this article, the validity of ideal ISM simplifications is studied by comparing the performances of an ISM system with idealized boundary conditions and a corresponding system with parallel nanochannels of charged walls. Assumptions of fixed voltage, fixed counter-ion concentration, and zero co-ion fluxes of the ideal ISM model are checked with the nanochannel systems using varied parameters of applied voltage, charge density, and the width and length of nanochannels. It is found that the ideal ISM model is capable of reproducing behaviors as the nanoporous, permselective membrane qualitatively, in terms of I–V curves and the ion concentration polarization effects. Through quantitative comparisons, it is demonstrated that the fixed voltage on the membrane surface is accurate under high electric field ($V > 5V_T$). The simplification of the fixed counter-ion concentration inside the ISM only holds under the condition that C_m is significantly higher than C_0 ($C_m \geq 5C_0$). However, zero co-ion flux is accurate only when the membrane is highly charged and the electric field is very low (without strong ICP). In addition, it is demonstrated that the effect of the sizes of nanopores in an ion selective membrane is trivial, as long as the pore size is smaller than the Debye length. The permselectivity of nanochannels increases with the channel lengths, meaning that the permselectivity of the ISM increases with the membrane's thickness. We believe that these findings will provide great guidance for future simulation calculation and help compare and analyze the results between simulation models and experiments.

ACKNOWLEDGMENTS

This work was supported by the National Natural Science Foundation of China (Grant Nos. 12072100 and 21576130) and the Kuwait Foundation for the Advancement of Sciences (Kuwait-MIT signature project, Project No. P31475EC01).

DATA AVAILABILITY

The data that support the findings of this study are available from the corresponding author upon reasonable request.

REFERENCES

[1] R. W. Baker, *Membrane Technology and Applications*, 2nd ed., Metallurgical Transactions A (Springer, 2004), https://www.springer.com/journal/11661.
[2] H. Strathmann, *Ion-Exchange Membrane Separation Processes* (Elsevier Science, Amsterdam, 2004), https://www.sciencedirect.com/bookseries/membrane-science-and-technology/vol/9.
[3] B. Kim, R. Kwak, H. J. Kwon, V. S. Pham, M. Kim, B. Al-Anzi, G. Lim, and J. Han, "Purification of high salinity brine by multi-stage ion concentration polarization desalination," Sci. Rep. **6**, 31850 (2016).
[4] J. Tang, L. Gong, J. Jiang, Z. Li, and J. Han, "Numerical simulation of electrokinetic desalination using microporous permselective membranes," Desalination **477**, 114262 (2020).
[5] S. J. Peighambardoust, S. Rowshanzamir, and M. Amjadi, "Review of the proton exchange membranes for fuel cell applications," Int. J. Hydrogen Energy **35**, 9349 (2010).
[6] H. Strathmann, A. Grabowski, and G. Eigenberger, "Ion-exchange membranes in the chemical process industry," Ind. Eng. Chem. Res. **52**, 10364 (2013).
[7] R. Kwak, S. J. Kim, and J. Han, "Continuous-flow biomolecule and cell concentrator by ion concentration polarization," Anal. Chem. **83**, 7348 (2011).
[8] T. Xu, "Ion exchange membranes: State of their development and perspective," J. Membr. Sci. **263**, 1 (2005).
[9] J. Schaep and C. Vandecasteele, "Evaluating the charge of nanofiltration membranes," J. Membr. Sci. **188**, 129 (2001).
[10] Q. Pu, J. Yun, H. Temkin, and S. Liu, "Ion-enrichment and ion-depletion effect of nanochannel structures," Nano Lett. **4**, 1099 (2004).
[11] A. H. Galama, J. W. Post, M. A. Stuart, and P. M. Biesheuvel, "Validity of the Boltzmann equation to describe Donnan equilibrium at the membrane–solution interface," J. Membr. Sci. **442**, 131 (2013).
[12] R. Parsons and R. Peat, "The adsorption of sucrose at the mercury-water interface," J. Electroanal. Chem. Interfacial Electrochem. **122**, 299 (1997).
[13] H. Chang and L. Y. Yeo, *Electrokinetically-Driven Microfluidics and Nanofluidics*, Electrostatics Electrodynamics, Vol. 13 (Cambridge University Press, 2008), http://assets.cambridge.org/97805218/60253/frontmatter/9780521860253_frontmatter.pdf.
[14] S. J. Kim, Y. C. Wang, J. H. Lee, H. Jang, and J. Han, "Concentration polarization and nonlinear electrokinetic flow near a nanofluidic channel," Phys. Rev. Lett. **99**, 044501 (2007).
[15] J. Wang, C. Liu, and Z. Xu, "Electrokinetic ion transport in confined micro-nanochannel," Electrophoresis **37**, 769 (2016).
[16] A. Campione, L. Gurreri, M. Ciofalo, G. Micale, A. Tamburini, and A. Cipollina, "Electrodialysis for water desalination. A critical assessment of recent developments on process fundamentals, models and applications," Desalination **434**, 121 (2018).

[17]J. G. D. Tadimeti and S. Chattopadhyay, "Uninterrupted swirling motion facilitating ion transport in electrodialysis," Desalination **392**, 54 (2016).
[18]R. Kwak, V. S. Pham, K. M. Lim, and J. Han, "Shear flow of an electrically charged fluid by ion concentration polarization: Scaling laws for electroconvective vortices," Phys. Rev. Lett. **110**, 114501 (2013).
[19]R. Kwak, G. Guan, W. K. Peng, and J. Han, "Microscale electrodialysis: Concentration profiling and vortex visualization," Desalination **308**, 138 (2013).
[20]E. Karatay, C. L. Druzgalski, and A. Mani, "Simulation of chaotic electrokinetic transport: Performance of commercial software versus custom-built direct numerical simulation codes," J. Colloid Interface Sci. **446**, 67 (2015).
[21]V. V. Nikonenko, S. A. Mareev, N. D. Pis'menskaya, A. M. Uzdenova, A. V. Kovalenko, and M. K. Urtenov, "Effect of electroconvection and its use in intensifying the mass transfer in electrodialysis (Review)," Russ. J. Electrochem. **53**, 1122 (2017).
[22]S. J. Kim, S. H. Ko, K. H. Kang, and J. Han, "Direct seawater desalination by ion concentration polarization," Nat. Nanotechnol. **5**, 297 (2010).
[23]V. V. Nikonenko, N. D. Pismenskaya, E. I. Belova, P. Sistat, P. Huguet, and P. Gerald, "Intensive current transfer in membrane systems: Modeling, mechanisms and application in electrodialysis," Adv. Colloid Interface Sci. **160**, 101 (2010).
[24]V. M. Barragán and C. Ruız-Bauzá, "Current–voltage curves for ion-exchange membranes: A method for determining the limiting current density," J. Colloid Interface Sci. **205**, 365 (1998).
[25]P. Malek, J. M. Ortiz, B. S. Richards, and A. I. Schäfer, "Electrodialytic removal of NaCl from water: Impacts of using pulsed electric potential on ion transport and water dissociation phenomena," J. Membr. Sci. **435**, 99 (2013).
[26]S. Alizadeh, M. Z. Bazant, and A. Mani, "A multiscale analysis of electrokinetic transport in porous media," in APS Meeting, 2017, https://ui.adsabs.harvard.edu/abs/2017APS..DFDD15001A/abstract.
[27]F. Maletzki, H. W. Rösler, and E. Staude, "Ion transfer across electrodialysis membranes in the overlimiting current range: Stationary voltage current characteristics and current noise power spectra under different conditions of free convection," J. Membr. Sci. **71**, 105 (1992).
[28]E. A. Demekhin, G. S. Ganchenko, and E. N. Kalaydin, "Transition to electrokinetic instability near imperfect charge-Selective membranes," Phys. Fluids **30**, 082006 (2018).
[29]A. Mani, T. A. Zangle, and J. G. Santiago, "On the propagation of concentration polarization from microchannel-nanochannel interfaces Part I: Analytical model and characteristic analysis," Langmuir **25**, 3898 (2009).
[30]R. Abu-Rjal, L. Prigozhin, I. Rubinstein, and B. Zaltzman, "Equilibrium electro-convective instability in concentration polarization: The effect of non-equal ionic diffusivities and longitudinal flow," Russ. J. Electrochem. **53**, 903 (2017).
[31]R. Abu-Rjal, I. Rubinstein, and B. Zaltzman, "Teorell instability in concentration polarization," Phys. Rev. E **92**, 022305 (2015).
[32]A. Uzdenova, A. Kovalenko, and M. Urtenov, "Theoretical analysis of the effect of ion concentration in solution bulk and at membrane surface on the mass transfer at overlimiting currents," Russ. J. Electrochem. **53**, 1254 (2017).
[33]V. V. Nikonenko, A. V. Kovalenko, M. K. Urtenov, N. D. Pismenskaya, J. Han, and P. Sistat, "Desalination at overlimiting currents: State-of-the-art and perspectives," Desalination **342**, 85 (2014).
[34]P. Magnico, "Spatial distribution of mechanical forces and ionic flux in electrokinetic instability near a permselective membrane," Phys. Fluids **30**, 014101 (2018).
[35]I. Rubinstein, B. Zaltzman, and I. Lerman, "Electroconvective instability in concentration polarization and nonequilibrium electro-osmotic slip," Phys. Rev. E **72**, 011505 (2005).
[36]I. Rubinstein and B. Zaltzman, "Electro-osmotically induced convection at a permselective membrane," Phys. Rev. E **62**, 2238 (2000).
[37]A. Mani and K. M. Wang, "Electroconvection near electrochemical interfaces: Experiments, modeling, and computation," Annu. Rev. Fluid Mech. **52**, 509 (2020).
[38]E. V. Dydek, B. Zaltzman, I. Rubinstein, D. S. Deng, A. Mani, and M. Z. Bazant, "Overlimiting current in a microchannel," Phys. Rev. Lett. **107**, 118301 (2011).
[39]I. Rubinstein and L. Shtilman, "Voltage against current curves of cation exchange membranes," J. Chem. Soc. Faraday Trans. **75**, 231–246 (1979).
[40]I. Rubinstein and B. Zaltzman, "Electro-convective versus electroosmotic instability in concentration polarization," Adv. Colloid Interface Sci. **134-135**, 190 (2007).
[41]I. Rubinstein and B. Zaltzman, "Extended space charge in concentration polarization," Adv. Colloid Interface Sci. **159**, 117 (2010).
[42]V. S. Pham, Z. Li, K. M. Lim, J. K. White, and J. Han, "Direct numerical simulation of electroconvective instability and hysteretic current-voltage response of a permselective membrane," Phys. Rev. E **86**, 046310 (2012).
[43]T. A. Zangle, A. Mani, and J. G. Santiago, "Effects of constant voltage on time evolution of propagating concentration polarization," Anal. Chem. **82**, 3114 (2010).
[44]M. Tedesco, H. V. M. Hamelers, and P. M. Biesheuvel, "Nernst-Planck transport theory for (reverse) electrodialysis: I. Effect of co-ion transport through the membranes," J. Membr. Sci. **510**, 370 (2016).
[45]I. Rubinstein and B. Zaltzman, "Equilibrium electroconvective instability," Phys. Rev. Lett. **114**, 114502-1 (2015).
[46]B. Zaltzman and I. Rubinstein, "Electro-osmotic slip and electroconvective instability," J. Fluid Mech. **579**, 173 (2007).
[47]A. Uzdenova and M. Urtenov, "Potentiodynamic and galvanodynamic regimes of mass transfer in flow-through electrodialysis membrane systems: Numerical simulation of electroconvection and current-voltage curve," Membranes **10**, 49 (2020).
[48]T. A. Zangle, A. Mani, and J. G. Santiago, "Theory and experiments of concentration polarization and ion focusing at microchannel and nanochannel interfaces," Chem. Soc. Rev. **39**, 1014 (2010).
[49]H. C. Chang, G. Yossifon, and E. A. Demekhin, "Nanoscale electrokinetics and microvortices: How microhydrodynamics affects nanofluidic ion flux," Annu. Rev. Fluid Mech. **44**, 401 (2012).
[50]Y. Green, S. Park, and G. Yossifon, "Bridging the gap between an isolated nanochannel and a communicating multipore heterogeneous membrane," Phys. Rev. E **91**, 011002 (2015).
[51]A. S. Rao, K. R. Rashimi, D. V. Manjunatha, A. Jayarama, and R. Pinto, "Pore size tuning of Nafion membranes by UV irradiation for enhanced proton conductivity for fuel cell applications," Int. J. Hydrogen Energy **42**, 23762 (2019).
[52]A.-C. Louër, A. Plecis, A. Pallandre, J.-C. Galas, A. Estevez-Torres, and A.-M. Haghiri-Gosnet, "Pressure-assisted selective preconcentration in a straight nanochannel," Anal. Chem. **85**, 7948 (2013).
[53]S. J. Kim, L. D. Li, and J. Han, "Amplified electrokinetic response by concentration polarization near nanofluidic channel," Langmuir **25**, 7759 (2009).
[54]M. Urtenov, A. Uzdenov, A. V. Kovalenkoa, V. V. Nikonenko, and G. Pourcelly, "Basic mathematical model of overlimiting transfer enhanced by electroconvection in flow-through electrodialysis membrane cells," J. Membr. Sci. **447**, 190 (2013).
[55]Z. R. Li, W. Liu, L. Y. Gong, D. Y. Zhu, Y. T. Gu, and J. Han, "Accurate multiphysics numerical analysis of particle preconcentration based on ion concentration polarization," Int. J. Appl. Mech. **9**(8), 1750107 (2017).
[56]I. Rubinstein and B. Zaltzman, "Electro-osmotic slip of the second kind and instability in concentration polarization at electrodialysis membranes," Math. Models Methods Appl. Sci. **11**, 263 (2001).